Phys. Lett. B 870 (2025) 139904

Contents lists available at ScienceDirect

Physics Letters B

journal homepage: www.elsevier.com/locate/physletb

Letter

First high-resolution in-beam γ-ray spectroscopy of neutron-rich Mo isotopes at relativistic energy

B. Moon [a,b,*], W. Korten [c], K. Wimmer [d,e,b,f], P. Doornenbal [b], T. R. Rodríguez [g], K. Yanase [b], T. Otsuka [b], N. Aoi [h], H. Baba [b], F. Browne [b], C. Campbell [i], S. Chen [j,k], Z. Chen [d], H. Crawford [i], H. De Witte [l], C. Fransen [m], H. Hess [m], E. Ideguchi [h], S. Iwazaki [h], J. Kim [n,o], N. Kitamura [p], A. Kohda [h], T. Koiwai [f], B. Mauss [b], R. Mizuno [f], M. Niikura [f], T. Parry [q], P. Reiter [m], H. Sakurai [b,f], D. Suzuki [b], R. Taniuchi [j], S. Thiel [m], Y. Yamamoto [h]

[a] Center for Exotic Nuclear Studies, Institute for Basic Science, Daejeon, 34126, Republic of Korea
[b] RIKEN Nishina Center, 2-1 Hirosawa, Wako, Saitama, 351-0198, Japan
[c] IRFU, CEA, Université Paris-Saclay, Gif-sur-Yvette, F-91191, France
[d] GSI Helmoltzzentrum für Schwerionenforschung GmbH, Planckstr. 1, Darmstadt, 64291, Germany
[e] Instituto de Estructura de la Materia, CSIC, Madrid, E-28006, Spain
[f] Department of Physics, University of Tokyo, 7-3-1 Hongo, Bunkyo, Tokyo, 113-0033, Japan
[g] Departamento de Estructura de la Materia, Física Térmica y Electrónica and IPARCOS, Universidad Complutense de Madrid, Madrid, 28040, Spain
[h] Research Center for Nuclear Physics (RCNP), Osaka University, Mihogaoka Ibaraki, Osaka, 567-0047, Japan
[i] Nuclear Science Division, Lawrence Berkeley National Laboratory, Berkeley, California, 94720, USA
[j] School of Physics, Engineering and Technology, University of York, Heslington, York, YO10 5DD, United Kingdom
[k] Department of Physics, The University of Hong Kong, Pokfulam, 999077, Hong Kong
[l] Institute for Nuclear and Radiation Physics, KU Leuven, Leuven, B-3001, Belgium
[m] Institut für Kernphysik, Universität zu Köln, Cologne, D-50937, Germany
[n] Department of Physics, Korea University, Seoul, 02841, Republic of Korea
[o] Center for Extreme Nuclear Matters, Korea University, Seoul, 02841, Republic of Korea
[p] Center for Nuclear Study, University of Tokyo, RIKEN campus, Wako, Saitama, 351-0198, Japan
[q] Department of Physics, University of Surrey, Guildford, GU2 7XH, United Kingdom

ARTICLE INFO

Editor: Prof. Betram Blank

Keywords:
Triaxial deformation
Mo isotopes
Lifetime measurement
In-beam γ-ray spectroscopy

ABSTRACT

High-resolution in-beam γ-ray spectroscopy of the neutron-rich $^{110}Mo_{68}$ and $^{112}Mo_{70}$ isotopes was performed for the first time at relativistic energies. This experiment was conducted at the Radioactive Isotope Beam Factory (RIBF), RIKEN. The ^{110}Mo and ^{112}Mo isotopes were produced via nucleon removal reactions of radioactive Mo and Tc ions, and the γ rays emitted following these reactions were measured using the High-resolution Cluster Array at RIBF (HiCARI). Doppler-corrected energy spectra enabled the precise determination of transition energies and half-lives through the line-shape method. In addition to providing new lifetime information, the level scheme of ^{112}Mo was extended, including the γ-band structure, and the precision of existing level energies was significantly improved. Using the lifetime data, reduced transition probabilities were deduced. The $B(E2;2_1^+ \to 0_1^+)$ values indicate large collectivity and deformation, while the properties of the 2_2^+ states and their decay to the ground-state band point to an increase in triaxial deformation from mid-shell toward $N = 70$. To interpret these findings, two theoretical models were applied and compared with the experimental results highlighting the importance of triaxial deformation.

The atomic nucleus serves as a fundamental system for exploring many-body quantum physics. While the nuclear shell model describes single-particle behaviour [1–3], the interplay of proton-proton, neutron-neutron, and proton-neutron interactions also gives rise to collective motion. The emergence of low-lying excited states in even-even nuclei, with energies below the nucleon pairing gap, was linked to nuclear collective motion by Rainwater [4] and further developed by Bohr and Mottelson [5] in the 1950s. In this framework, an axially symmetric deformed nucleus exhibits a rotational ground-state band, while β and γ vibrations correspond to oscillations along different axes.

* Corresponding author.
E-mail addresses: mb0316@ibs.re.kr (B. Moon), w.korten@cea.fr (W. Korten), k.wimmer@gsi.de (K. Wimmer).

https://doi.org/10.1016/j.physletb.2025.139904
Received 4 April 2025; Received in revised form 16 June 2025; Accepted 18 September 2025
Available online 21 September 2025

While the conventional collective model effectively describes many nuclei, some require additional degrees of freedom. Triaxial deformation, characterised by the γ degree of freedom ranging from 0° (prolate) to 60° (oblate), accounts for such cases. While quadrupole deformation and rotation are reflected in the properties of the ground-state band, this triaxial motion is closely linked to the γ band, built on an excited 2^+_γ state. With increasing γ deformation, the excitation energy of the 2^+_γ state is reduced.To describe triaxial deformation, Davydov and Filippov introduced the rigid triaxial rotor model [6]. Assuming static maximum triaxiality of $\gamma = 30°$, this model predicts the 2^+_γ state at lower excitation energy than the 4^+_1 state and its main decay branch to proceed to the 2^+_1 state. In contrast, the γ-unstable rotor model proposed by L. Wilets and M. Jean assumes no strict confinement of γ in the potential energy surface [7]. In this case, the model predicts the degeneracy of the 4^+_1 and 2^+_2 states.

Neutron-rich Mo isotopes are key candidates for studying triaxiality. Beyond-mean-field calculations with the Gogny D1S interaction predict ground-state triaxial deformation in ^{102}Mo–^{110}Mo [8] and the density functional theory (UNEDF0) suggests triaxiality in ^{106}Mo and ^{108}Mo [9]. Experimental efforts over decades have focused on γ-band structures to probe triaxiality in these isotopes [10–13]. Recent studies on ^{106}Mo, ^{108}Mo, and ^{110}Mo have combined advanced theoretical approaches with empirical models, including γ-band energy staggering patterns [14]. However, interpretations vary, emphasizing different aspects such as γ vibration, rigid triaxial rotors, and γ-unstable behaviour. This underscores the need for more precise experimental data, particularly reduced transition probabilities, to refine our understanding of triaxiality in exotic nuclei.

In this letter, we report lifetime measurements of excited states in neutron-rich ^{110}Mo and ^{112}Mo using the Doppler-broadened line-shape method at relativistic energies [15]. In particular, the lifetimes of the 2^+_x states, except the 2^+_1 state in ^{110}Mo, were measured for the first time in this region, which are sensitive to triaxiality. Additionally, we present a significantly revised level scheme for ^{112}Mo, including more precise transition energies. The experimental results are then compared with state-of-the-art nuclear model calculations, providing new insights into the structure of these isotopes.

The experiment was carried out at the Radioactive Isotope Beam Factory (RIBF) at RIKEN where a cocktail beam was produced via in-flight fission of a ^{238}U primary beam impinging on a 4-mm-thick ^{9}Be target at an energy of 345 AMeV. The fission fragments were selected and identified using the BigRIPS spectrometer, employing the $B\rho - \Delta E$-Time-of-Flight method [16,17]. In a secondary reaction, ^{110}Mo was produced by one-neutron removal from ^{111}Mo on a 6-mm-thick ^{9}Be target at approximately 235 AMeV, while ^{112}Mo was generated via one-proton removal from ^{113}Tc. In each case the isotope of interest was transmitted through the ZeroDegree Spectrometer and identified using the same method as in BigRIPS. The γ rays emitted following the removal reactions were detected with the High-resolution Cluster Array at RIBF (HiCARI) [18]. To optimise detection efficiency and sensitivity for longer lifetimes of several hundred picoseconds, the secondary ^{9}Be target was positioned 10-cm upstream of the HiCARI focal point. Six Miniball triple-cluster detectors [19] were mounted at forward angles, covering angles from 15° to 35° with respect to the beam axis. Four segmented clover detectors [20] were installed to cover the angle range of 38° − 65° together with two modules of GRETINA-type tracking detectors [21]. Doppler correction was performed under the assumption that the interaction point with the highest energy deposit corresponded to the first photon interaction within the detector material. For the tracking detectors, the interaction points were determined using signal decomposition, as detailed in [22]. For the segmented detectors, the segment centres were used, based on the average of first interactions derived from simulations. Precise detector positioning within the laboratory system was achieved using photogrammetry measurements. The clover-type detectors were excluded from the analysis due to their limited sensitivity to long lifetimes arising from the large polar angles relative to the beam direction.

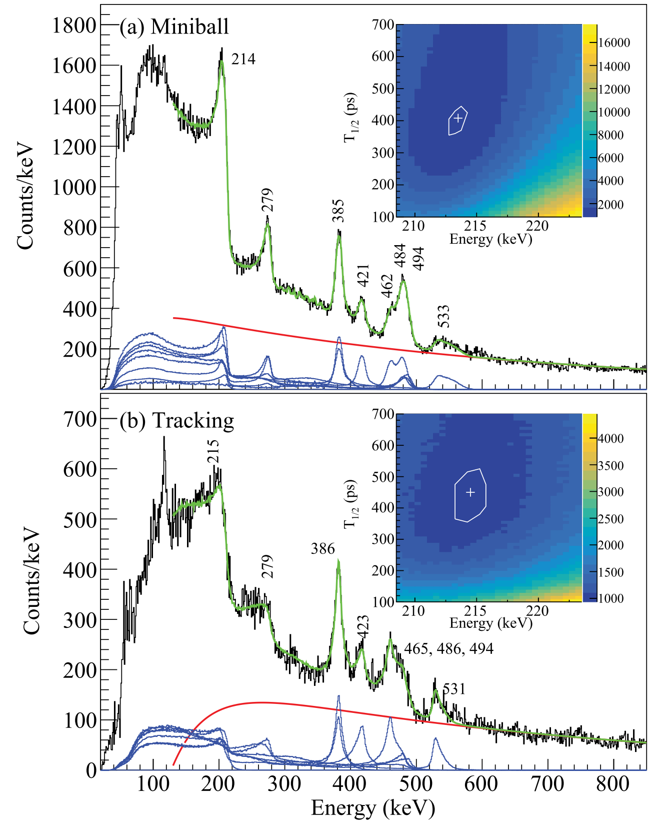

Fig. 1. Doppler-corrected energy spectra of ^{110}Mo, after atomic background subtraction, measured by (a) the Miniball detectors and (b) the tracking detectors. The data are superimposed by a fit result (green lines) obtained by adding the simulated individual response functions (blue lines) and a continuous background (red lines). The insets show the χ^2 maps of the $2^+_1 \rightarrow 0^+_1$ transitions obtained by varying combinations of transition energy and half-life. The minimum χ^2 values are marked with white crosses and white contours indicate the area where energy and half-life simultaneously take on values within the 1σ range of the optimum values. Transitions are labelled with the γ-ray energies extracted from the fits of individual detector groups. (For interpretation of the references to color in this figure legend, the reader is referred to the web version of this article.)

The detection efficiencies of the Miniball and tracking detectors (for γ-ray emission at rest) were approximately 1.5 % and 1.3 % at 0.3 MeV, respectively.

Figs. 1 and 2 show Doppler-corrected energy spectra of ^{110}Mo and ^{112}Mo, respectively. As described in [23], the Doppler correction was applied using the velocity of the ions after the target as most decays occur behind the target, based on a mean transit time of approximately 35 ps. Naturally, this leads to some distortion for fast transitions such as the $6^+ \rightarrow 4^+$ transitions around 530 keV. Additionally, the atomic background was removed following the method described in [23]. To extract transition energies and half-lives, the response functions of all individual detectors for each excited state were reproduced using a customised simulation package [24] based on the Geant4 framework [25]. The key difference from the previous work [23] is that the feeding or cascading effects from higher-lying levels could be fully incorporated, as the internal level structure of ^{110}Mo has been well established through decay spectroscopy, providing precise energy and relative intensity information [14]. For ^{112}Mo, this feeding effect could be also incorporated assuming, however, the similarity in the γ-ray transition patterns as in ^{110}Mo. The total response functions of the Miniball and tracking detectors for decay cascades are shown as blue lines in Figs. 1 and 2 for ^{110}Mo and ^{112}Mo, respectively.

Table 1
Summary of level excitation energies, transition energies, level half-lives, spin assignments, and reduced transition probabilities in ^{110}Mo and ^{112}Mo obtained from the present work. Those results are mean values obtained from the Miniball and tracking detectors. Uncertainties include both statistical and systematic errors (1 keV for energies and 10 % for half-lives). The theoretical $B(E2)$ values from the SCCM [29] and QVSM [30] calculations are given for comparison.

E_{level} (keV)	E_γ (keV)	$T_{1/2,\ \text{level}}$ (ps)	J_i^π	J_f^π	$B(E2;\ J_i^\pi \to J_f^\pi)$ (e^2b^2)		
^{110}Mo$_{68}$					This work [a]	SCCM	QVSM
$214.1^{+1.8}_{-1.9}$	$214.1^{+1.8}_{-1.9}$	430^{+69}_{-70}	(2_1^+)	0_1^+	$0.28^{+0.05}_{-0.04}$	0.28	0.27
$493.2^{+2.5}_{-2.6}$	$279.1^{+1.8}_{-1.8}$	146^{+30}_{-33}	(2_2^+)	(2_1^+)	$0.11^{+0.04}_{-0.02}$ [b]	0.39	0.06
–	$493.2^{+1.8}_{-1.8}$	–	(2_2^+)	0_1^+	$0.006^{+0.002}_{-0.001}$ [b]	1.4×10^{-3}	0.03
$599.7^{+3.0}_{-3.1}$	$385.6^{+1.7}_{-1.8}$	26^{+7}_{-8}	(4_1^+)	(2_1^+)	$0.26^{+0.11}_{-0.05}$	0.41	0.39
$699.2^{+3.8}_{-4.0}$	$206.0^{+2.0}_{-2.4}$	62^{+19}_{-15}	(3_1^+)	(2_2^+)	$0.57^{+0.20}_{-0.14}$ [b]	0.51	0.50
–	$485.1^{+2.0}_{-2.4}$	–	(3_1^+)	(2_1^+)	$0.025^{+0.006}_{-0.009}$ [b]	4×10^{-5}	0.05
$915.0^{+4.7}_{-5.2}$	$421.8^{+1.8}_{-2.1}$	51^{+11}_{-15}	(4_2^+)	(2_2^+)	$0.08^{+0.03}_{-0.02}$	0.17	0.18
$1131.9^{+3.8}_{-4.0}$	$532.2^{+2.3}_{-2.6}$	$3.5^{+2.3}_{-2.2}$	(6_1^+)	(4_1^+)	$0.38^{+0.61}_{-0.15}$	0.52	0.45
$1162.9^{+5.2}_{-5.7}$	$463.7^{+2.3}_{-2.3}$	20^{+7}_{-8}	(5_1^+)	(3_1^+)	$0.14^{+0.09}_{-0.04}$	0.30	0.30
^{112}Mo$_{70}$					This work [a]	SCCM	QVSM
$241.1^{+1.9}_{-1.8}$	$241.1^{+1.9}_{-1.8}$	234^{+40}_{-43}	(2_1^+)	0_1^+	$0.28^{+0.06}_{-0.05}$	0.17	0.30
$518.7^{+2.9}_{-2.7}$	$277.6^{+2.2}_{-2.1}$	158^{+35}_{-36}	(2_2^+)	(2_1^+)	$0.14^{+0.05}_{-0.03}$ [c]	0.16	0.17
–	$518.7^{+2.2}_{-2.1}$	–	(2_2^+)	0_1^+	$0.003^{+0.011}_{-0.001}$ [c]	0.02	0.02
$655.1^{+3.5}_{-3.4}$	$414.0^{+2.1}_{-2.1}$	30^{+14}_{-11}	(4_1^+)	(2_1^+)	$0.15^{+0.15}_{-0.05}$	0.27	0.45
$747.6^{+5.3}_{-5.4}$	$506.5^{+2.3}_{-2.5}$	47^{+17}_{-16}	(3_1^+)	(2_1^+)	$0.04^{+0.02}_{-0.01}$	0.03	0.04
$991.7^{+5.7}_{-5.9}$	$473.0^{+2.1}_{-2.5}$	42^{+17}_{-17}	(4_2^+)	(2_2^+)	$0.06^{+0.04}_{-0.02}$	0.22	0.16
$1215.7^{+4.8}_{-4.8}$	$560.6^{+3.3}_{-3.3}$	$2.8^{+1.8}_{-2.2}$	(6_1^+)	(4_1^+)	$0.36^{+0.68}_{-0.14}$	0.37	0.54

[a] All transitions are assumed to have pure $E2$ character.
[b] Using the $B(E2)$ ratios from [14].
[c] Using the $B(E2)$ ratios from [28].

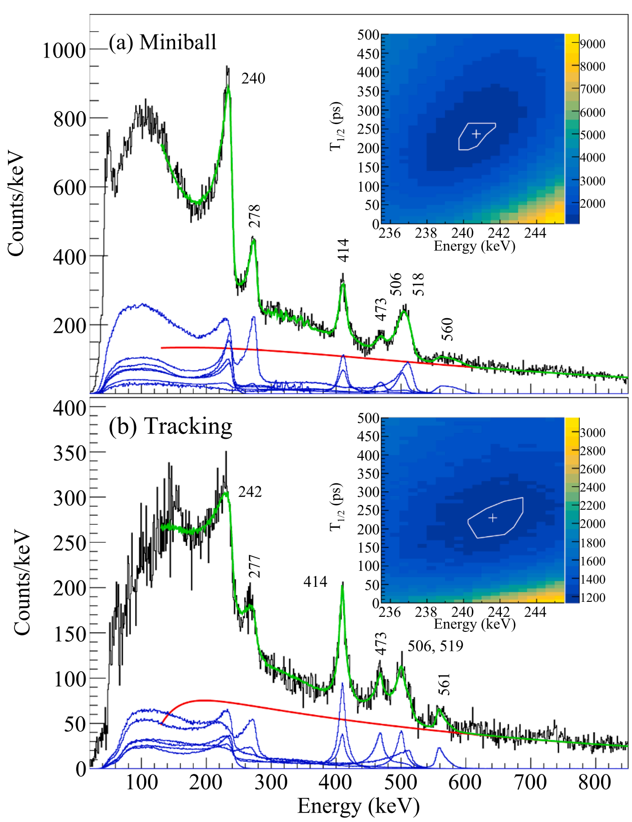

Fig. 2. Same as Fig. 1 but for the ^{112}Mo case.

The response functions were varied in 0.5-keV steps for the transition energies of all excited states in the simulation. For the lifetimes, 5-ps steps were used for the long-lived (2_1^+) and (2_2^+) states, and 2-ps steps for all other excited states. The Doppler-corrected energy spectra were fitted using these response functions including a continuous background comprising of two exponential functions. The fits were evaluated using two-dimensional χ^2 maps, as shown in the insets of Figs. 1 and 2. The mean values and 1σ uncertainties for transition energies and half-lives were extracted from these χ^2 maps, after smoothing the χ^2 surface and following the procedure detailed in [23]. The white crosses in the χ^2 maps indicate the optimum $E - T_{1/2}$ combinations corresponding to the minimum $\chi^2 = \chi^2_{\text{min}}$. The white solid lines represent $\chi^2_{\text{min}} + 2.4$ contours, denoting region where the probability of both energy and half-life values lies within one standard deviation, thus taking into account correlated uncertainties [23,26]. Excitation energies and decay half-lives were extracted for the two detector groups individually and in all cases consistent results were obtained independently. The final fit results, as weighted averages of the two detector groups, are shown as green lines in Figs. 1 and 2, and the extracted optimal fit values are summarised in Table 1. Besides the statistical uncertainties extracted from the χ^2 maps, systematic errors were added, which are primarily attributable to uncertainties in the target position, the velocity of the projectile-like fragments, and angular positions of detectors. The first two factors cause a systematic error of approximately 1 keV in energy, while 10 % of the systematic error was applied to the measured half-lives to compensate the variation between different angle groups.

For ^{110}Mo, all measured energies are consistent between the detector groups and with previous results [14]. All half-lives, except for the $(2_1^+) \to 0_1^+$ transition, were newly measured in the present work. Notably, our measured half-life of the $(2_1^+) \to 0_1^+$ transition, 430^{+69}_{-70} ps, is considerably shorter than the previously reported value of 582(28) ps [14]. This inconsistency can be attributed to the difference of the experimental method, the level populations, and feeding effects in the β-decay experiment. The apparent differences in the response function intensities at 490 keV between the Miniball and tracking detectors can be attributed to the differing lifetime sensitivities of these detector types. Miniball detectors are significantly more sensitive to longer lifetimes, and the 486- and 494-keV transitions exhibit comparatively longer half-lives than the 464-keV transition. As a result, the peak heights of the 486- and 494-keV transitions appear more pronounced in Miniball detectors, while the tail structures are more extended in the tracking detectors.

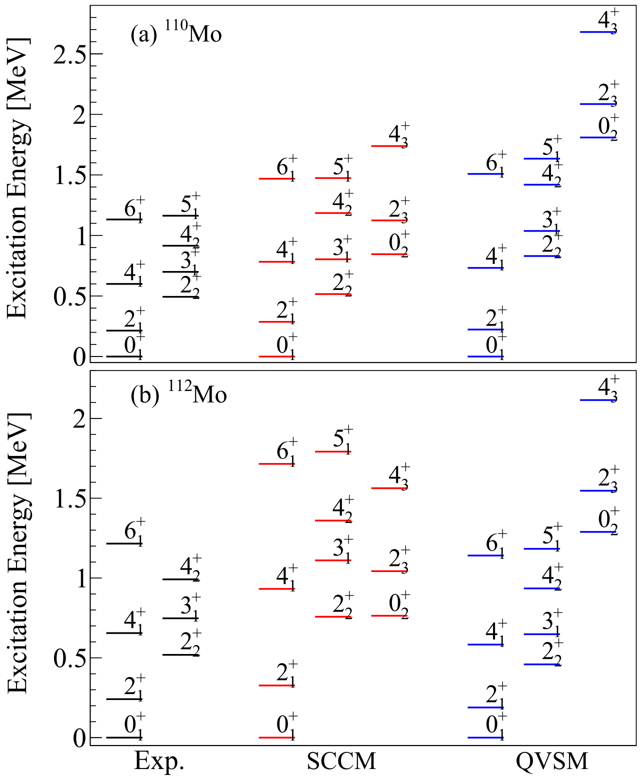

Fig. 3. Level schemes obtained from the present work (black) and theoretical predictions using the SCCM [29] (red) and QVSM [30] (blue) interactions for (a) ^{110}Mo and (b) ^{112}Mo, respectively. The 0_2^+-state band structures are represented for the theoretical predictions, which could not be observed from the current data. (For interpretation of the references to color in this figure legend, the reader is referred to the web version of this article.)

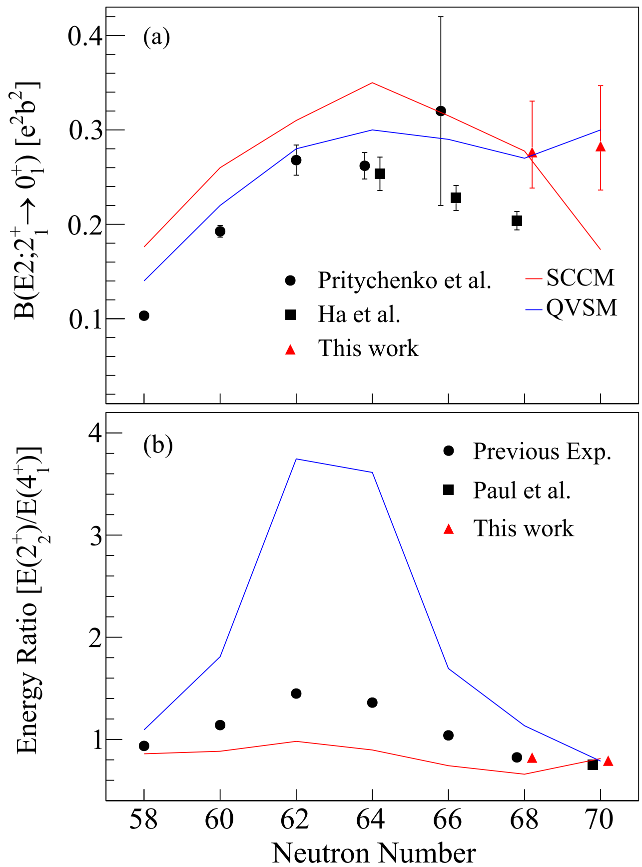

Fig. 4. Systematic plot of (a) reduced transition probabilities and (b) energy ratios between 4_1^+ and 2_2^+ states in Mo isotopes as a function of neutron number. Theoretical results from the SCCM [29] and QVSM [30] calculations are shown to compare with the experimental data [14,27,35,36].

In ^{112}Mo, all half-lives were newly measured, and the level scheme was significantly extended compared to the previous work [27]. Since statistics were not sufficient for the construction of $\gamma-\gamma$ coincidences, the level scheme of ^{112}Mo was established based on the γ-ray energy sum method and comparison with the neighbour ^{110}Mo. A new transition at 278 keV was clearly identified, and the triplet structure at approximately 500 keV could be resolved, in contrast to the previous work [27]. The excitation energies of the (2_1^+), (4_1^+), and (2_2^+) states could be more precisely measured as $241.1^{+1.9}_{-1.8}$, $655.1^{+3.5}_{-3.4}$, and $518.7^{+2.9}_{-2.7}$ keV, respectively, compared to previous values of 235(7), 645(12), and 485(26) keV. Furthermore, transitions from the (6_1^+), (3_1^+), and (4_2^+) states were newly observed, and with the latter two, for the first time, a γ-band structure was established in ^{112}Mo. The half-life of the $(2_1^+)\rightarrow 0_1^+$ transition was determined to be 234^{+40}_{-43} ps. Moreover, the half-life of the 2_2^+ state was measured as 158^{+35}_{-36} ps, which is very similar to ^{110}Mo. To deduce the $B(E2)$ values from the (2_2^+) state to the ground and (2_1^+) states the newly measured branching ratio was applied [28]. The other measured half-lives are also very similar, leading to a good agreement between the $B(E2)$ values determined for ^{110}Mo and ^{112}Mo, as summarised in Table 1. In particular, the $B(E2)$ values for the (2_1^+) and (2_2^+) states exhibit quasi identical values.

It is worth emphasising that, as shown in Fig. 3, the level structures of ^{110}Mo and ^{112}Mo are very similar; however, the deformation in the ground-state band appears to decrease when evaluated through the 2_1^+ excitation energies and the energy ratios between 4_1^+ and 2_1^+, with $E(4_1^+)/E(2_1^+) = 2.80$ and 2.72 for ^{110}Mo and ^{112}Mo, respectively.

Fig. 4(a) presents the systematics of reduced transition probabilities $B(E2; 2_1^+ \rightarrow 0_1^+)$ values for the neutron-rich Mo isotopes. The new data points suggest that the $B(E2; 2_1^+ \rightarrow 0_1^+)$ values may start to saturate starting from $N = 64$. Furthermore, the relative position of the 2_2^+ state with respect to the 4_1^+ state, shown as their ratio in Fig. 4(b), strongly decreases from $N = 62$ onwards, suggesting that the triaxial deformation increases with neutron number. However, between ^{110}Mo and ^{112}Mo the measured $B(E2; 2_2^+ \rightarrow 2_1^+)$ and $B(E2; 2_2^+ \rightarrow 0_1^+)$ values stay constant within their uncertainties indicating persisting strong triaxial deformation towards $N = 70$. The observed $E(4_1^+)/E(2_1^+)$ and $E(2_2^+)/E(2_1^+)$ ratios in ^{110}Mo and ^{112}Mo are consistent with γ values of 25.5° and 27°, respectively, when applying the rigid triaxial rotor model [6]. However, applying these γ values to determine the $B(E2; 2_2^+ \rightarrow 2_1^+)$ values, yields larger values of 0.27 and 0.33 e^2b^2, as compared to the experimental ones of $0.11^{+0.04}_{-0.02}$ and $0.14^{+0.05}_{-0.03}$ e^2b^2 for ^{110}Mo and ^{112}Mo, respectively, indicating that the interpretation as rigid triaxial rotation is not sufficient.

To describe the experimental findings two different theoretical models have been employed. The first is the symmetry-conserving configuration-mixing (SCCM) method [29] with the Gogny D1S interaction [31,32]. In this version of a beyond-mean-field approach, a set of quadrupole-deformed, angular-momentum and particle-number projected Hartree-Fock-Bogolyubov (HFB) states is generated by minimising the particle-number projected energy under constraints imposed on the quadrupole degrees of freedom (Q_0, Q_2) related to the deformation parameters (β_2, γ). The final nuclear states are described as linear combinations of these projected intrinsic states within the generator coordinate framework. Thanks to the so-called collective wave functions, this method enables the interpretation of individual nuclear states in terms of the probability of certain axial and triaxial shapes.

The total energy surfaces in the (β_2, γ) plane, calculated using the Gogny D1S interaction, exhibit a similar structure in both isotopes with a relatively smooth minimum extending from $(0.35, 25°)$ to $(0.25, 60°)$. More details on the calculations will be presented in a forthcoming publication [33]. After angular momentum projection and configuration mixing, the ground-state band of the ^{110}Mo nucleus is predominantly built from triaxial configurations around $(0.35, 25°)$, whereas in ^{112}Mo the deformation is slightly smaller and shifts towards a more oblate shape, $(0.30, 40°)$. In addition, $\Delta J = 1$ bands, built upon a 2_2^+ state, is predicted. Their collective wave functions are also triaxial, peaking around $(0.35, 25°)$ in both isotopes. Additionally, a second $\Delta J = 2$ band appears at relatively low excitation energies, characterised by minimal mixing between the oblate and triaxial states presented in the energy surface. These bands are yet to be identified experimentally. The calculated bands appear stretched compared to the experimental results. Performing angular momentum projection before variation and/or including cranked states in the initial set of states mixed within the SCCM method would reduce this effect [34], however, this is beyond the scope of the present work.

Regarding the transition probabilities, $B(E2; 2_1^+ \to 0_1^+)$, the SCCM calculations with the Gogny-D1S interaction exhibit an inverted parabolic trend between ^{100}Mo and ^{112}Mo, as shown in Fig. 4(a). This is consistent with the experimental data for the $^{100-108}$Mo interval, although the calculated values are systematically higher due to the overestimation of the deformation. Finally, the SCCM calculations predict rather γ-soft energy surfaces throughout the entire isotopic chain. Correspondingly, the ratios $E(2_2^+)/E(4_1^+)$ remain fairly constant and close to 1. As shown in Fig. 4(b), the experimental values of these ratios are slightly higher, which could indicate a more rigid triaxial rotational behaviour. It is also worth noting that the $B(E2; 2_2^+ \to 2_1^+)/B(E2; 2_1^+ \to 0_1^+)$ ratios obtained from the SCCM calculations decrease in ^{112}Mo and in fact the γ degree of freedom changes from $\gamma = 25°$ to $40°$. However, these ratios are in both cases overestimated compared to the experimental results (see Table 1).

The second model employed to describe the experimental observations is the Quasiparticle Vacua Shell Model (QVSM), which represents the most advanced methodology in Monte-Carlo Shell Model calculations, utilising particle-number, angular momentum, and parity projected, quasiparticle vacua as basis vectors, rather than Slater determinants [30]. For ^{110}Mo, the predicted 2_1^+ excitation energy and the $B(E2; 2_1^+ \to 0_1^+)$ value agree well with experimental results, but the energy ratios of $E(4_1^+)/E(2_1^+) = 3.28$ and $E(2_2^+)/E(4_1^+) = 1.13$ are overestimated. On the other hand, the $B(E2; 2_2^+ \to 2_1^+)$ and $B(E2; 2_2^+ \to 0_1^+)$ values, which are sensitive to the triaxial deformation, are also consistent with the measured values. The T-plot [37] for this isotope shows prolate-triaxial deformation with γ softness in the ground state centred at $\gamma \approx 20°$ [33]. For ^{112}Mo, the predicted level spectrum in Fig. 3(b) fits well with the experimental results. Furthermore, the $B(E2)$ values for the 2_1^+ and 2_2^+ states are also consistent with the experimental findings. The lowering of the 2_2^+ state in ^{112}Mo in conjunction with the increased $B(E2; 2_2^+ \to 2_1^+)/B(E2; 2_1^+ \to 0_1^+)$ ratio suggests that this isotope exhibits increased triaxiality, which is also supported by T-plot minimum at $\gamma \approx 25°$.

Interestingly, the QVSM calculation predicts a further increase in collectivity for $N = 70$, a trend that differs not only from the SCCM model, but also from the results for the Zr isotopes discussed in [23]. However, due to the large experimental uncertainties in the $B(E2; 2_1^+ \to 0_1^+)$ values, it remains to be clarified whether collectivity in Mo isotopes is indeed enhanced at $N = 70$. Finally, as can be seen in Fig. 4(b) the QVSM predicts a very large $E(2_2^+)/E(4_1^+)$ ratio around $N = 64$, which is not observed experimentally and opposite to the SCCM predictions. Neither of the models seems to fully capture the evolution of triaxial deformation along the isotopic chain.

The QVSM model also predicts shape coexistence in both ^{110}Mo and ^{112}Mo with an oblate deformed excited 0_2^+ state. As shown in Fig. 3, the 0_2^+ states exhibit rotational band structures, but located at higher energy than in the SCCM. In ^{112}Mo, this structure is expected at a lower excitation energy, although it remains much higher than the SCCM prediction. Candidates for 0_2^+ states in ^{110}Mo and ^{112}Mo have not yet been identified.

By comparing with two different models, we conclude that the most neutron-rich Mo isotopes accessible experimentally, ^{110}Mo and ^{112}Mo, exhibit similar structural characteristics consistent with significant triaxial deformation in their ground states. Our data support the importance of triaxiality in these isotopes, but a clear distinction between rigid and soft requires further investigations. These new findings go beyond the results of a previous study, which proposed axial symmetry in the ground state, mainly based on excitation energies and backed by five-dimensional collective Hamiltonian calculations with Skyrme interactions [14].

In summary, we performed the first high-resolution in-beam γ-ray spectroscopy of ^{110}Mo and ^{112}Mo at RIBF using the HiCARI system. In this experiment, we measured the half-lives of excited states in both nuclei and established new levels in ^{112}Mo. The newly determined level scheme and reduced transition probabilities for ^{112}Mo closely match those of ^{110}Mo, suggesting a smooth evolution of nuclear shape and collectivity in the Mo isotopes towards $N = 70$. In particular, the newly measured transition rates of the 2_x^+ states enabled us to confirm the importance of strong triaxial deformation, in general accordance with the predictions from the SCCM and QVSM model calculations. While shape coexistence with a higher-lying, oblate-deformed structure is also predicted by both models, these structures were not observed in this experiment. Future studies with a high-efficiency γ-ray tracking array will be needed to verify these predictions and to clearly establish the exact nature of nuclear deformation in this mass region.

This work was carried out at the RIBF operated by RIKEN Nishina Center and Center for Nuclear Study in the University of Tokyo. We acknowledge the Miniball Collaboration for the loan of the Miniball detectors and supporting frame. Research Center for Nuclear Physics in Japan, Institute of Modern Physics in China, and Lawrence Berkeley National Laboratory and Argonne National Laboratory in USA are also acknowledged for the loan of the detectors and data acquisition electronics. The HiCARI campaign was supported by the JSPS KAKENHI of Japan under the Grant Nos. Kiban-A JP19H00670 and JP19H01914. B. Moon acknowledges supports from Institute for Basic Science (IBS) (Grant No. IBS-R031-Y1) and National Research Foundation (NRF) (Grant No. 2019R1A6A3A03031564) of the Republic of Korea. K. Wimmer acknowledges funding from the Spanish Ministerio de Ciencia, Innovación y Universidades (Grant No. RYC-2017-22007) and the European Research Council (ERC) under the European Union's Horizon 2020 research and innovation programme (grant agreement No. 101001561). T. R. Rodríguez acknowledges funding from the Spanish MICIN under contract PID2021-127890NB-I00 and support from GSI-Darmstadt computing facilities. F. Browne acknowleges a support from the Special Postdoctoral Researcher program of RIKEN. S. Chen and R. Taniuchi were supported by the Royal Society and the UK STFC under Grant numbers ST/P003885/1, ST/V001035/1, and ST/Y000285/1. J. Kim acknowledges a support from NRF of the Republic of Korea under Grant No. 2018R1A5A1025563. P. Reiter acknowledges funding from the German BMBF under contracts 05P18PKCIA and 'Verbundprojekt' 05P21PKCI1.

Data availability

Data will be made available on request.

Declaration of competing interest

The authors declare the following financial interests/personal relationships which may be considered as potential competing interests:

B. Moon reports financial support was provided by Institute for Basic Science. B. Moon reports financial support was provided by National Research Foundation of Korea. K. Wimmer reports financial support was provided by Spanish Ministerio de Ciencia, Innovación y Universidades.

K. Wimmer reports financial support was provided by European Research Council. T. R. Rodriguez reports financial support was provided by Spanish MICIN. T. R. Rodriguez reports equipment, drugs, or supplies was provided by GSI Helmholtz Centre for Heavy Ion Research GmbH. F. Browne reports financial support was provided by RIKEN. S. Chen reports financial support was provided by The Royal Society. R. Taniuchi reports financial support was provided by The Royal Society. S. Chen reports financial support was provided by UK STFC. R. Taniuchi reports financial support was provided by UK STFC. J. Kim reports financial support was provided by National Research Foundation of Korea. P. Reiter reports financial support was provided by German BMBF. B. Moon reports equipment, drugs, or supplies was provided by RIKEN Nishina Center for Accelerator-Based Science. B. Moon reports equipment, drugs, or supplies was provided by Center for Nuclear Study, University of Tokyo. B. Moon reports equipment, drugs, or supplies was provided by Research Center for Nuclear Physics Osaka University. B. Moon reports equipment, drugs, or supplies was provided by Miniball Collaboration. B. Moon reports equipment, drugs, or supplies was provided by Institute of Modern Physics Chinese Academy of Sciences. B. Moon reports equipment, drugs, or supplies was provided by E O Lawrence Berkeley National Laboratory. B. Moon reports equipment, drugs, or supplies was provided by Argonne National Laboratory. K. Wimmer reports financial support was provided by JSPS. D. Suzuki reports financial support was provided by JSPS. If there are other authors, they declare that they have no known competing financial interests or personal relationships that could have appeared to influence the work reported in this paper.

References

[1] M.G. Mayer, Phys. Rev. 74 (1948) 235–239.
[2] M.G. Mayer, Phys. Rev. 75 (1949) 1969–1970.
[3] O. Haxel, J.H.D. Jensen, H.E. Suess, Phys. Rev. 75 (1949) 1766–1766.
[4] J. Rainwater, Phys. Rev. 79 (1950) 432–434.
[5] A. Bohr, B.R. Mottelson, Mat. Fys. Medd. K. Dan. Vid. Selsk. 27 (1953) 16.
[6] A.S. Davydov, G.F. Filippov, Nucl. Phys. 8 (1958) 237–249.
[7] L. Wilets, M. Jean, Phys. Rev. 102 (1956) 788–796.
[8] J.P. Delaroche, M. Girod, J. Libert, H. Goutte, S. Hilaire, S. Péru, N. Pillet, G.F. Bertsch, Phys. Rev. C 81 (2010) 014303.
[9] C.L. Zhang, G.H. Bhat, W. Nazarewicz, J.A. Sheikh, Y. Shi, Phys. Rev. C 92 (2015) 034307.
[10] A. Guessous, N. Schulz, W.R. Phillips, I. Ahmad, M. Bentaleb, J.L. Durell, M.A. Jones, M. Leddy, E. Lubkiewicz, L.R. Morss, R. Piepenbring, A.G. Smith, W. Urban, B.J. Varley, Phys. Rev. Lett. 75 (1995) 2280–2283.
[11] A. Guessous, N. Schulz, M. Bentaleb, E. Lubkiewicz, J.L. Durell, C.J. Pearson, W.R. Phillips, J.A. Shannon, W. Urban, B.J. Varley, I. Ahmad, C.J. Lister, L.R. Morss, K.L. Nash, C.W. Williams, S. Khazrouni, Phys. Rev. C 53 (1996) 1191–1196.
[12] K. Shizuma, H. Lawin, K. Sistemich, Zeitschrift für Physik A Atoms and Nuclei 311 (1) (1983) 71–78.
[13] H. Watanabe, K. Yamaguchi, A. Odahara, T. Sumikama, S. Nishimura, K. Yoshinaga, Z. Li, Y. Miyashita, K. Sato, L. Próchniak, H. Baba, J.S. Berryman, N. Blasi, A. Bracco, F. Camera, J. Chiba, P. Doornenbal, S. Go, T. Hashimoto, S. Hayakawa, C. Hinke, N. Hinohara, E. Ideguchi, T. Isobe, Y. Ito, D.G. Jenkins, Y. Kawada, N. Kobayashi, Y. Kondo, R. Krücken, S. Kubono, G. Lorusso, T. Nakano, T. Nakatsukasa, M. Kurata-Nishimura, H.J. Ong, S. Ota, Z. Podolyák, H. Sakurai, H. Scheit, K. Steiger, D. Steppenbeck, K. Sugimoto, K. Tajiri, S. Takano, A. Takashima, T. Teranishi, Y. Wakabayashi, P.M. Walker, O. Wieland, H. Yamaguchi, Phys. Lett. B 704 (4) (2011) 270–275.
[14] J. Ha, T. Sumikama, F. Browne, N. Hinohara, A.M. Bruce, S. Choi, I. Nishizuka, S. Nishimura, P. Doornenbal, G. Lorusso, P.A. Söderström, H. Watanabe, R. Daido, Z. Patel, S. Rice, L. Sinclair, J. Wu, Z.Y. Xu, A. Yagi, H. Baba, N. Chiga, R. Carroll, F. Didierjean, Y. Fang, N. Fukuda, G. Gey, E. Ideguchi, N. Inabe, T. Isobe, D. Kameda, I. Kojouharov, N. Kurz, T. Kubo, S. Lalkovski, Z. Li, R. Lozeva, H. Nishibata, A. Odahara, Z. Podolyák, P.H. Regan, O.J. Roberts, H. Sakurai, H. Schaffner, G.S. Simpson, H. Suzuki, H. Takeda, M. Tanaka, J. Taprogge, V. Werner, O. Wieland, Phys. Rev. C 101 (2020) 044311.
[15] P. Doornenbal, P. Reiter, H. Grawe, T. Saito, A. Al-Khatib, A. Banu, T. Beck, F. Becker, P. Bednarczyk, G. Benzoni, A. Bracco, A. Bürger, L. Caceres, F. Camera, S. Chmel, F.C.L. Crespi, H. Geissel, J. Gerl, M. Górska, J. Grębosz, H. Hübel, M. Kavatsyuk, O. Kavatsyuk, M. Kmiecik, I. Kojouharov, N. Kurz, R. Lozeva, A. Maj, S. Mandal, W. Meczynski, B. Million, Z. Podolyák, A. Richard, N. Saito, H. Schaffner, M. Seidlitz, T. Striepling, J. Walker, N. Warr, H. Weick, O. Wieland, M. Winkler, H.J. Wollersheim, Nucl. Instrum. Methods Phys. Res. 613 (2) (2010) 218–225.
[16] T. Kubo, D. Kameda, H. Suzuki, N. Fukuda, H. Takeda, Y. Yanagisawa, M. Ohtake, K. Kusaka, K. Yoshida, N. Inabe, T. Ohnishi, A. Yoshida, K. Tanaka, Y. Mizoi, Prog. Theor. Exp. Phys. 2012 (1) (2012) 03C003.
[17] N. Fukuda, T. Kubo, T. Ohnishi, N. Inabe, H. Takeda, D. Kameda, H. Suzuki, Nucl. Instrum. Methods Phys. Res. 317 (2013) 323–332.
[18] K. Wimmer, P. Doornenbal, N. Aoi, H. Baba, F. Browne, C. Campbell, H. Crawford, H. De Witte, C. Fransen, H. Hess, S. Iwazaki, J. Kim, A. Kohda, T. Koiwai, B. Mauss, B. Moon, T. Parry, P. Reiter, D. Suzuki, R. Taniuchi, S. Thiel, Y. Yamamoto, RIKEN Accel. Prog. Rep. 54 (2021) S27.
[19] N. Warr, J. Van de Walle, M. Albers, F. Ames, B. Bastin, C. Bauer, V. Bildstein, A. Blazhev, S. Bönig, N. Bree, B. Bruyneel, P.A. Butler, J. Cederkäll, E. Clément, T.E. Cocolios, T. Davinson, H. De Witte, P. Delahaye, D.D. DiJulio, J. Diriken, J. Eberth, A. Ekström, J. Elseviers, S. Emhofer, D.V. Fedorov, V.N. Fedosseev, S. Franchoo, C. Fransen, L.P. Gaffney, J. Gerl, G. Georgiev, R. Gernhäuser, T. Grahn, D. Habs, H. Hess, A.M. Hurst, M. Huyse, O. Ivanov, J. Iwanicki, D.G. Jenkins, J. Jolie, N. Kesteloot, O. Kester, U. Köster, M. Krauth, T. Kröll, R. Krücken, M. Lauer, J. Leske, K.P. Lieb, R. Lutter, L. Maier, B.A. Marsh, D. Mücher, M. Münch, O. Niedermaier, J. Pakarinen, M. Pantea, G. Pascovici, N. Patronis, D. Pauwels, A. Petts, N. Pietralla, R. Raabe, E. Rapisarda, P. Reiter, A. Richter, O. Schaile, M. Scheck, H. Scheit, G. Schrieder, D. Schwalm, M. Seidlitz, M. Seliverstov, T. Sieber, H. Simon, K.H. Speidel, C. Stahl, I. Stefanescu, P.G. Thirolf, H.G. Thomas, M. Thürauf, P. Van Duppen, D. Voulot, R. Wadsworth, G. Walter, D. Weißhaar, F. Wenander, A. Wiens, K. Wimmer, B.H. Wolf, P.J. Woods, K. Wrzosek-Lipska, K.O. Zell, Eur. Phys. J. A 49 (2013) 40.
[20] W. Hua, N.T. Zhang, M.L. Liu, Y. Zheng, Y.D. Fang, X.H. Zhou, Y.H. Zhang, X.G. Lei, Y.X. Guo, Nucl. Struct. China 2012 (2013) 98–100.
[21] D. Weisshaar, D. Bazin, P.C. Bender, C.M. Campbell, F. Recchia, V. Bader, T. Baugher, J. Belarge, M.P. Carpenter, H.L. Crawford, M. Cromaz, B. Elman, P. Fallon, A. Forney, A. Gade, J. Harker, N. Kobayashi, C. Langer, T. Lauritsen, I.Y. Lee, A. Lemasson, B. Longfellow, E. Lunderberg, A.O. Macchiavelli, K. Miki, S. Momiyama, S. Noji, D.C. Radford, M. Scott, J. Sethi, S.R. Stroberg, C. Sullivan, R. Titus, A. Wiens, S. Williams, K. Wimmer, S. Zhu, Nucl. Instrum. Methods Phys. Res. 847 (2017) 187–198.
[22] S. Paschalis, I.Y. Lee, A.O. Macchiavelli, C.M. Campbell, M. Cromaz, S. Gros, J. Pavan, J. Qian, R.M. Clark, H.L. Crawford, D. Doering, P. Fallon, C. Lionberger, T. Loew, M. Petri, T. Stezelberger, S. Zimmermann, D.C. Radford, K. Lagergren, D. Weisshaar, R. Winkler, T. Glasmacher, J.T. Anderson, C.W. Beausang, Nucl. Instrum. Methods Phys. Res. 709 (2013) 44–55.
[23] B. Moon, W. Korten, K. Wimmer, P. Doornenbal, T.R. Rodríguez, N. Aoi, H. Baba, F. Browne, C. Campbell, S. Chen, H. Crawford, H. de Witte, C. Fransen, H. Hess, E. Ideguchi, S. Iwazaki, J. Kim, N. Kitamura, A. Kohda, T. Koiwai, B. Mauss, R. Mizuno, M. Niikura, T. Parry, P. Reiter, H. Sakurai, D. Suzuki, R. Taniuchi, S. Thiel, Y. Yamamoto, Phys. Lett. B 858 (2024) 139047.
[24] K. Wimmer, UCHiCARI, 2019 (https://www.nishina.riken.jp/collaboration/SUNFLOWER/devices/hrarray).
[25] S. Agostinelli, J. Allison, K. Amako, J. Apostolakis, H. Araujo, P. Arce, M. Asai, D. Axen, S. Banerjee, G. Barrand, F. Behner, L. Bellagamba, J. Boudreau, L. Broglia, A. Brunengo, H. Burkhardt, S. Chauvie, J. Chuma, R. Chytracek, G. Cooperman, G. Cosmo, P. Degtyarenko, A. Dell'Acqua, G. Depaola, D. Dietrich, R. Enami, A. Feliciello, C. Ferguson, H. Fesefeldt, G. Folger, F. Foppiano, A. Forti, S. Garelli, S. Giani, R. Giannitrapani, D. Gibin, J.J. Gómez Cadenas, I. González, G. Gracia Abril, G. Greeniaus, W. Greiner, V. Grichine, A. Grossheim, S. Guatelli, P. Gumplinger, R. Hamatsu, K. Hashimoto, H. Hasui, A. Heikkinen, A. Howard, V. Ivanchenko, A. Johnson, F.W. Jones, J. Kallenbach, N. Kanaya, M. Kawabata, Y. Kawabata, M. Kawaguti, S. Kelner, P. Kent, A. Kimura, T. Kodama, R. Kokoulin, M. Kossov, H. Kurashige, E. Lamanna, T. Lampén, V. Lara, V. Lefebure, F. Lei, M. Liendl, W. Lockman, F. Longo, S. Magni, M. Maire, E. Medernach, K. Minamimoto, P. Mora de Freitas, Y. Morita, K. Murakami, M. Nagamatu, R. Nartallo, P. Nieminen, T. Nishimura, K. Ohtsubo, M. Okamura, S. O'Neale, Y. Oohata, K. Paech, J. Perl, A. Pfeiffer, M.G. Pia, F. Ranjard, A. Rybin, S. Sadilov, E. Di Salvo, G. Santin, T. Sasaki, N. Savvas, Y. Sawada, S. Scherer, S. Sei, V. Sirotenko, D. Smith, N. Starkov, H. Stoecker, J. Sulkimo, M. Takahata, S. Tanaka, E. Tcherniaev, E. Safai Tehrani, M. Tropeano, P. Truscott, H. Uno, L. Urban, P. Urban, M. Verderi, A. Walkden, W. Wander, H. Weber, J.P. Wellisch, T. Wenaus, D.C. Williams, D. Wright, T. Yamada, H. Yoshida, D. Zschiesche, Nucl. Instrum. Methods Phys. Res. 506 (3) (2003) 250–303.
[26] F. James, MINUIT Function Minimization and Error Analysis Reference Manual, 1994 (https://root.cern.ch/download/minuit.pdf).
[27] N. Paul, A. Corsi, A. Obertelli, P. Doornenbal, G. Authelet, H. Baba, B. Bally, M. Bender, D. Calvet, F. Château, S. Chen, J.P. Delaroche, A. Delbart, J.-M. Gheller, A. Giganon, A. Gillibert, M. Girod, P.H. Heenen, V. Lapoux, J. Libert, T. Motobayashi, M. Niikura, T. Otsuka, T.R. Rodríguez, J.Y. Roussé, H. Sakurai, C. Santamaria, N. Shimizu, D. Steppenbeck, R. Taniuchi, T. Togashi, Y. Tsunoda, T. Uesaka, T. Ando, T. Arici, A. Blazhev, F. Browne, A.M. Bruce, R. Carroll, L.X. Chung, M.L. Cortés, M. Dewald, B. Ding, F. Flavigny, S. Franchoo, M. Górska, A. Gottardo, A. Jungclaus, J. Lee, M. Lettmann, B.D. Linh, J. Liu, Z. Liu, C. Lizarazo, S. Momiyama, K. Moschner, S. Nagamine, N. Nakatsuka, C. Nita, C.R. Nobs, L. Olivier, Z. Patel, Z. Podolyák, M. Rudigier, T. Saito, C. Shand, P.A. Söderström, I. Stefan, R. Orlandi, V. Vaquero, V. Werner, K. Wimmer, Z. Xu, Phys. Rev. Lett. 118 (2017) 032501.
[28] T. Sumikama, J. Ha, 2025 (in a private communication.).
[29] L.M. Robledo, T.R. Rodríguez, R.R. Rodríguez-Guzmán, J. Phys. G 46 (2019) 013001.
[30] N. Shimizu, Y. Tsunoda, Y. Utsuno, T. Otsuka, Phys. Rev. C 103 (2021) 014312.
[31] J. Dechargé, D. Gogny, Phys. Rev. C 21 (1980) 1568–1593.
[32] J.F. Berger, M. Girod, D. Gogny, Comput. Phys. Commun. 63 (1) (1991) 365–374.
[33] B. Moon, et al. (to be published.).
[34] M. Borrajo, T.R. Rodríguez, J. Luis Egido, Phys. Lett. B 746 (2015) 341–346.
[35] B. Pritychenko, M. Birch, B. Singh, M. Horoi, Atom. Data Nucl. Data Tab. 107 (2016) 1–139.
[36] National Nuclear Data Center, Brookhaven National Laboratory, 2025 (http://www.nndc.bnl.gov).
[37] Y. Tsunoda, T. Otsuka, N. Shimizu, M. Honma, Y. Utsuno, Phys. Rev. C 89 (2014) 031301.